



# Study on the effect of raindrops on the dynamic stall of a NACA-0012 airfoil

Armin Sheidani<sup>1</sup> · Sajad Salavatidezfouli<sup>2</sup> · Paolo Schito<sup>1</sup>

Received: 26 July 2021 / Accepted: 27 March 2022 / Published online: 24 April 2022  
© The Author(s) 2022, corrected publication 2022

## Abstract

In this study the pure effect of raindrops on dynamic stall of a pitching airfoil has been investigated. The simulation was performed at Reynolds number of  $10^6$  with raindrop diameter equal to  $10^{-5}$  m. A couple of multiphase models based on Eulerian and Lagrangian frames of reference have been implemented to simulate the raindrops. In the first step the accuracy of each multiphase model has been appraised. As a result, the Lagrangian multiphase model, which is called Discrete Phase Model, has been proven to be of better accuracy. It has been concluded that in general raindrops has negative effects on the lift coefficient of the pitching airfoil. In addition, a lead in aerodynamic phenomena has been observed due to the presence of water drops. This phenomenon has also been observed in the formation and separation of Leading Edge and Trailing Edge vortices which come to existence in advance of the dry case. Finally, it has been illustrated that the main effect of raindrops is on the phase of force oscillation rather than the force amplitude.

**Keywords** Pitching airfoil · Rain · Dynamic stall · Discrete phase model (DPM) · Dispersed multiphase (DMP)

## List of symbols

$L$	Lift force magnitude (N)	Re	Reynolds number $\rho Uc/\mu$
$D$	Drag force magnitude (N)	We	Weber number $\rho U^2 l/\sigma$
$A$	Reference area surface ( $m^2$ )	$f$	Frequency of pitching motion (Hz)
$C_L$	Lift coefficient $L/0.5\rho AU^2$	$f_r$	Drag function
$C_D$	Drag Coefficient $D/0.5\rho AU^2$	$t$	Time (s)
$c$	Airfoil chord (m)	$T$	Period of pitching motion (s)
$C_c$	Slip correction factor	$k$	Reduced frequency
$m_p$	Particle mass (kg)	$\theta$	Airfoil angle (degree)
$d_p$	Particle diameter (m)	$\rho$	Density ( $kg/m^3$ )
$g_x$	Gravity ( $m/s^2$ )	$\mu$	Dynamic viscosity (Pa.s)
$\tau_r$	Relaxation time (s)	$\alpha$	Mass fraction of water
$U$	Velocity magnitude (m/s)	$\nu$	Kinematic viscosity ( $m^2/s$ )

Technical Editor: André Cavalieri.

✉ Armin Sheidani  
armin.sheidani@polimi.it  
Sajad Salavatidezfouli  
ssalavat@sissa.it  
Paolo Schito  
paolo.schito@polimi.it

<sup>1</sup> Department of Mechanical Engineering, Politecnico di Milano, Milan, Italy

<sup>2</sup> Mathematics Area, MathLab, International School for Advanced Studies (SISSA), Trieste, Italy

## 1 Introduction

Owing to their vast industrial applications, pitching motion and dynamic stall behavior of airfoils have been of great interest to many researchers. To illustrate, output power of wind turbines could be controlled either by pitch to feather or stall where the latter, as the name suggests, brings about dynamic stall on the blade [1, 2]. Furthermore, airplane maneuver, MAVs motion and turbomachines performance are highly affected by dynamic stall. As a result, in the last decades some theoretical [3–5], experimental [6–9] and

numerical [10–14] attempts have been made to investigate dynamic stall.

Many researchers attempted to investigate different aspects of dynamic stall through understanding effects of geometrical parameters [15–17], turbulence [18–20] and vortex structures formation [20, 21]. For instance, Visbal and Garmann [22] studied the dynamic stall of a 3-D wing by the employment of large eddy simulation (LES) method. It was shown that before the formation of the dynamic stall vortex (DSV) a laminar separation bubble (LSB) appears on the leading edge of the airfoil.

Due to the fact that stall leads to a drop in the lift coefficient and the subsequent detrimental effects, postponement of flow separation by various control methods has been a topic of interest for the researchers in this field as well. Active flow controllers like synthetic jets and plasma as well as passive controllers have been studied for dynamic stall control in recent years owing to their high performance [23–30]. In a study, Tadjfar and Asgari [31] attempted to find the optimal location of a synthetic jet. It was reported that at optimum location the drag coefficient decreased significantly. It was found that the employment of synthetic jets at lower frequencies delays the dynamic stall better compared to higher amplitudes.

Rain as a sporadic meteorological phenomenon could impose penalties to the aerodynamic efficiency of an airborne device which cannot be thoroughly considered in the design process. As a result, the investigation of rain effect on the aerodynamic characteristics has been an ongoing issue explained in different studies. For instance, the work of Rhode [32], Luers [33] and Hess and Spectron [34] could be regarded as the first attempts to shed light to the physics of rain and air flow interaction. In the following years, Bezos et al. [35, 36] performed an experimental study on the effect of raindrop on the aerodynamic performance of an airfoil under heavy rain condition. Thompson et al. [37] derived the correlation between the surface-film behavior and aerodynamic coefficients for a wing with a NACA-4412 airfoil profile by means of experimental methods. It should be noted with the advances in the computational resources, numerical techniques began to be implemented to describe the physics of raindrop on the aerodynamic behavior of an airborne. The Eulerian–Lagrangian method is the general framework of modelling raindrops in the literature which will be discussed in details in the following sections. In this regard, the study conducted by Valentine and Decker [38] is one of the very first attempts to numerically simulate the raindrop effect on an airfoil. Wu et al. [39], Wu and Cao [40] and Ismail et al. [41] also implemented a numerical study to find the penalty in the aerodynamic coefficients as a result of the raindrops and the airfoil interaction. Fatahian et al. [42, 43] studied the performance of gurney flaps and slatted

airfoils under rainy condition. In another study, Fatahian et al. [44] investigated the effect of rain on aeroacoustics behavior of an airfoil employing Volume of Fluid (VOF), an Eulerian–Eulerian approach, for the film formation on the airfoil, along with Eulerian–Lagrangian reference of frame to take the raindrops into consideration. It should be noted that there is a common finding in the literature that indicates the presence of rain leads to a decrease in the aerodynamic performance of an airfoil. Another aspect of rainy condition which needs to be taken care of with more details is on airfoils utilized in energy production machines e.g., wind turbines. Cai et al. [45] developed a Eulerian–Lagrangian method to study the performance of a wind turbine airfoil under rainy condition. It was reported that the two-phase model successfully simulated the rain effect on the airfoil and the results suggested a considerable penalty on the aerodynamic performance. Aiden and Arastoopour [46] studied the effect of rain and the water-film formation on the aerodynamic performance of an airfoil of a wind turbine blade by Discrete Phase Model (DPM) and Volume of Fluid (VOF), respectively. It should be noted that DPM is a Eulerian–Lagrangian method which solves the discrete phase in the Lagrangian frame of reference moving along with the particles e.g., raindrops, and the primary phase is solved in the stationary frame of reference known as Eulerian. Wu et al. [47] investigated the effect of rain on the performance of vertical axis wind turbine. Similar to the previous studies, it was demonstrated that the presence raindrops leads to the exacerbation of aerodynamic performance the wind turbine. Nevertheless, airfoil has not been the only topic of interest for researchers. To illustrate, Jian et al. [48] investigated the effect of rain drop on the liquid film thickness formed on the windshield of a train. Yu et al. [49] investigated the aerodynamics of an Ahmet body under heavy rain condition.

Generally, most of the research in this field focused on the dynamic stall in the dried conditions, and moreover, the raindrop investigations were mainly aimed to understand the physics of static aerodynamic bodies. However, moving airborne devices, such as pitching airfoil, may undergo dynamic stall in the rainy conditions as well. Having considered the studies conducted so far, one comes to this conclusion that the effect of raindrops on the characteristics of the dynamic stall, which is very common in real life applications of this phenomenon, has remained unnoticed. In fact, the presence of raindrops in the upstream flow can affect the aerodynamic loads and flow characteristics downstream of the pitching airfoil. Due to the presence of the raindrops which adds more momentum to the upstream flow, and also considering the interaction between the raindrops and the turbulent flow structures, some variations in flow characteristics compared to the baseline case could be expected. In

the following sections, the effect of the rainy condition on the dynamic stall of a NACA-0012 airfoil and the mechanisms leading to aerodynamic characteristics variation will be investigated by means of numerical methods namely, two-phase flow methods and turbulence modelling technique.

## 2 Problem description

In this study the effect of the rain on flow characteristics over a pitching airfoil oscillating around its one quarter chord in dynamic stall condition has been numerically investigated by means of Ansys Fluent v18. It should be noted that the geometry and the pitching were set according to that of [24]. The oscillating airfoil is a NACA-0012 profile with a chord length of 0.58 m which has been subjected to a uniform flow with the inlet velocity being equal to 24.93 (m/s). Therefore, the mentioned parameters result in a Reynolds number equal to  $10^6$ . In addition, the NACA-0012 airfoil undergoes a sinusoidal motion according to Eq. 1 as follows:

$$\theta = \theta_0 + A\sin(2\pi ft) \tag{1}$$

where  $\theta_0$  is the initial incidence angle of the airfoil being equal to  $14.98^\circ$ . Moreover,  $A$  is the amplitude of the motion which was set to be 10 degrees. As a result, the amplitude of the airfoil fluctuation ranges from  $4.98^\circ$  to  $24.98^\circ$ . Also,  $f$  is the frequency of motion however, as demonstrated in the literature, reduced frequency, which is denoted by  $k$ , is preferred to frequency as it also takes the free stream velocity into consideration which leads to a more thorough description of the motion. Reduced frequency is calculated by Eq. 2 and it should be mentioned that for this study its value was considered to be equal to 0.15.

$$k = \frac{\pi fc}{U_\infty} \tag{2}$$

In addition, because the main non-dimensional number ruling the physics of incompressible flows is the Reynolds number, this number was set to be equal for both the dry and rainy cases. The parameter which needs to be adjusted to make the Reynolds number of the wet and dry cases equal is the inlet velocity as the density and viscosity for both the wet and dry cases are obtained by equations as follows:

$$\rho = \alpha \cdot \rho_{\text{water}} + (1 - \alpha) \cdot \rho_{\text{air}} \tag{3}$$

$$\mu = \alpha \cdot \mu_{\text{water}} + (1 - \alpha) \cdot \mu_{\text{air}} \tag{4}$$

where  $\alpha$ ,  $\rho$  and  $\mu$  are the mass fraction of water, density, and viscosity, respectively. The simulation was decided to be performed at a relatively low amount of liquid water content

to avoid much difference in the inlet velocity as this study is intended to take the effect of the waterdrops into consideration only. Therefore, the water liquid content was set to  $2.1 \text{ g/m}^3$  as suggested in [34]. The lift and drag coefficients were calculated, respectively, based on the density obtained from Eq. 3 as presented in Eqs. 5–6. It should be noted that the vertical relative velocity component of raindrops was neglected to study the pure effect of drops interacting with the airfoil and the airflow. The role of the vertical relative velocity component could be investigated in future studies.

Obviously, the mass fraction of water for the dry case was set to zero.

$$C_L = L/0.5\rho U_\infty^2 A \tag{5}$$

$$C_D = D/0.5\rho U_\infty^2 A \tag{6}$$

where  $L$  and  $D$  correspond to lift and drag force magnitude, respectively. Also, the reference area as denoted by  $A$ , is the surface of a rectangle which is parallel to the flow confined to the chord and span lines of the airfoil.

## 3 Numerical method

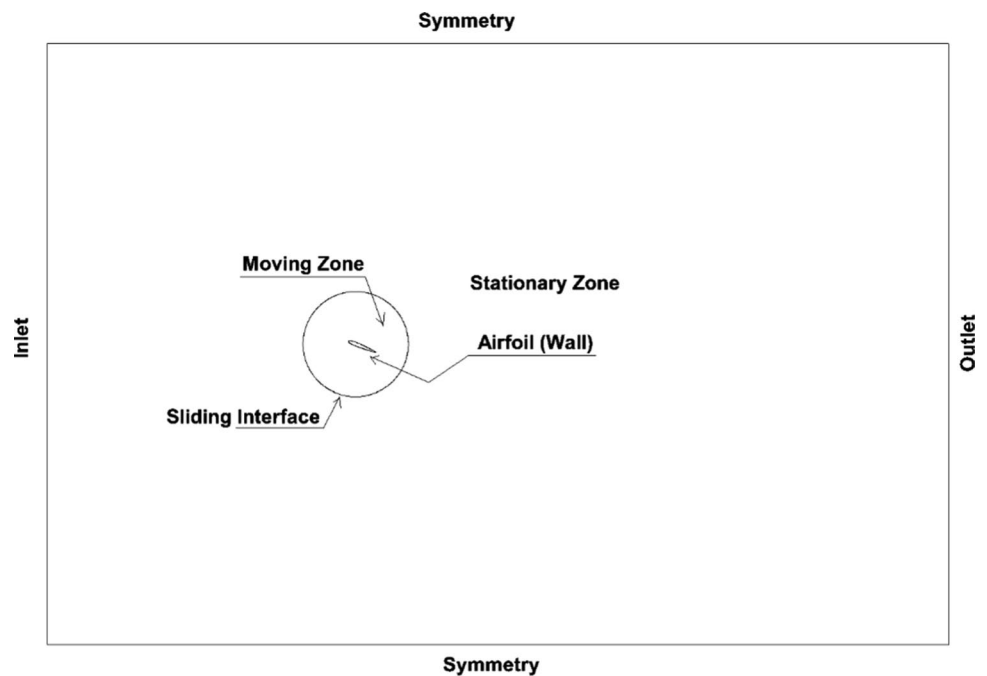
Considering the fact that the Reynolds number lies in the range of turbulent flow regime, 2-D unsteady Reynolds averaged Navier–Stokes (URANS) presented in Eq. 7 was numerically solved by ANSYS FLUENT Version 18.0 commercial code.

$$\frac{\partial U_i}{\partial t} + U_j \frac{\partial U_j}{\partial x_j} = -\frac{1}{\rho} \frac{\partial P}{\partial x_i} + \frac{\partial}{\partial x_j} \left( \frac{\mu}{\rho} \frac{\partial U_i}{\partial x_j} \right) + \frac{\partial (-u'_i u'_j)}{\partial x_j} \tag{7}$$

To solve Eq. 7  $k-\omega$  Shear–Stress Transport (SST) method was utilized owing to its widely known capabilities in precisely localizing the separation and also predicting the flow characteristics both in pre- and post-stall condition. This method, i.e.,  $k-\omega$  SST, is a two-equation URANS model which solves the region in the vicinity of the wall by standard  $k-\omega$  turbulence model, while the flow variables of the far field region are obtained by  $k-\epsilon$  model, thanks to their capabilities in predicting the boundary layer separation and the free stream characteristics, respectively. In order for the turbulence modelling equation to be able to switch from  $k-\omega$  to  $k-\epsilon$  interchangeably, it is multiplied by a blending function whose value is considered to be one in the near wall and null in the far field region.

The boundary conditions applied to the systems of equations has been presented in Fig. 1. The airfoil surface was considered to be wall with no-slip condition. In addition, at the upper and lower bounds of the numerical domain, as seen

**Fig. 1** Boundary condition and zone names in the numerical domain



in Fig. 1, the gradients of all the variables were assumed to be zero. This boundary condition has been specified as “symmetry” as shown in Fig. 1. Moreover, to impose pitching motion to the airfoil, the domain has been decomposed into two separate regions called inner and outer region. It should be mentioned that the pitching motion was imposed to the inner region using the sliding mesh technique. As a result, no mesh stretching/compression and mesh destruction/generation was employed which makes the solution far more accurate. Also, note that the type of the surrounding circle is “interface” meaning that conservation of the flux of flow variables on either side of the boundary would be guaranteed. For solving mentioned equations, a pressure-based solver using SIMPLE pressure–velocity coupling was implemented. In addition, all the spatial and temporal terms in the equations presented above were discretized by second order upwind and second order method. In addition, least square cell base method was employed to discretize the gradients.

To take the effect of raindrops into consideration, two multiphase models which were DPM and Dispersed Multiphase (DMP), which is a Eulerian–Eulerian method which models a dispersed phase (rain) in a primary phase (air) both in a stationary frame of reference, were employed. DPM is a Lagrangian–Eulerian method which regards the primary phase i.e., the phase whose volume fraction is far more dominating than that of the other phase, to be solved by Eulerian approach. As a result, the primary phase flow field is obtained by working out Eq. 7 presented earlier. Further, in DPM, the behavior of secondary phase, which is the phase with considerably lower amount of volume fraction, is described by Lagrangian approach. To predict the trajectory

of the secondary phase, the resulting force acting on the particles needs to be calculated and by striking the force balance, the inertial force will be equal to the force exerted by the primary phase. As a result, Eq. 8 presented below will be the governing equation of the Lagrangian equation whose result specifies the particles trajectories.

$$m_p \frac{du_p}{dt} = m_p \frac{(u - u_p)}{\tau_r} + \frac{g_x(\rho_p - \rho)}{\rho_p} + F_x \quad (8)$$

where the first term on the right-hand side of the equation above is the drag force, and  $F_x$  represents additional forces acting on the particles. It should be noted that  $\tau_r$  is the drop-let or particle relaxation time obtained as follows:

$$\tau_r = \frac{\rho_p d_p^2}{18\mu f_r} \quad (9)$$

A further discussion of the relaxation time is found in Sect. 4.4.

Many attempts have been made to present a relationship between the drag function,  $f_r$ , and the primary flow characteristics. Nevertheless, Schiller and Naumann correlation has been employed in this study to predict the drag function:

$$f_r = \frac{C_D Re}{24} \quad (10)$$

where

$$C_D = \begin{cases} 24(1 + 0.15\text{Re}^{0.687}), & \text{Re} < 1000 \\ 0.44, & \text{Re} \geq 1000 \end{cases} \quad (11)$$

In Discrete Phase Model (DPM) it is assumed that the dispersed phase, which possesses a lower amount of volume fraction, has been scattered throughout the flow field. DPM, unlike DPM, includes an Euler–Euler system of equation. In addition, in each cell the volume fraction is obtained through the continuity equation. On the other hand, the continuity equation needs to be calculated for each phase. As a result, the set of equations for DPM are as follows:

$$\frac{\partial}{\partial t} \int_V \alpha_i \rho_i dV + \oint_A \alpha_i \rho_i v_i \cdot da = 0 \quad (12)$$

$$\frac{\partial}{\partial t} \int_V \alpha_i \rho_i v_i dV + \oint_A \alpha_i \rho_i v_i \times v_i \cdot da = - \int_V \alpha_i \nabla p dV + F_{ij}^D \quad (13)$$

where  $\alpha_i$ ,  $\rho_i$  and  $v_i$  are volume fraction, density and velocity component of the dispersed phase  $i$ . Moreover,  $F_{ij}^D$  is the drag forced exerted by the primary phase to the dispersed phase  $j$ . Also,  $p$  stands for the static pressure which includes the buoyancy force.

## 4 Parameters independency and validation

To verify the performance and the choice of numerical parameters in the numerical simulation the parameters affecting the results need to be thoroughly investigated. The parameters which are going to be studied in this section are mesh and time step independency, numerical solution validation against experimental results and multiphase accuracy. Having performed the mentioned studies, one may ensure the validity of the numerical solution to draw reasonable conclusions in the following sections.

### 4.1 Mesh independency

To investigate the sensitivity of the numerical solution to the mesh size, three different meshes with 50,000, 150,000 and 250,000 cells were generated and the variation of lift and drag coefficient with the mesh size is plotted in Fig. 2. It is evident in Fig. 2 that after 1,50,000 cells the variation in lift and drag coefficients is less than one percent. Therefore, the mesh with 1,50,000 cells was selected to perform the further numerical simulations on it. Moreover, the value of  $y^+$  was calculated all over the airfoil and its maximum number is 1.8. In Fig. 3 the graphical and qualitative presentation of the mesh generated around the airfoil can be observed. It should

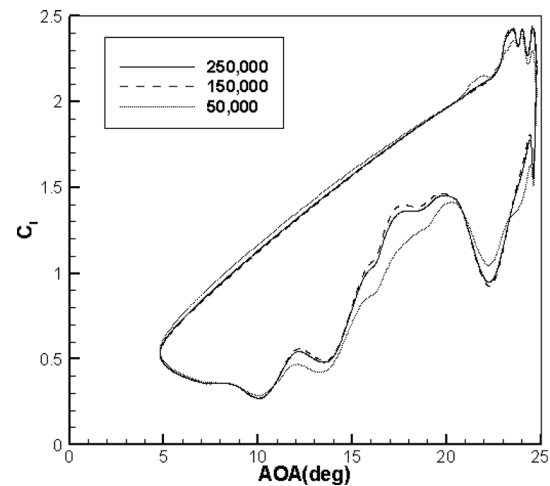


Fig. 2 Mesh independency study

be noted that the Angle of Attack (AOA) has been presented in degrees in all the figures of this paper.

### 4.2 Time step independency

To implement time step independency study, three different time steps were considered. The time step size was determined with respect to the amount of time the airfoil needs to sweep one period of the oscillating movement. As a result, considering the angular velocity of the airfoil, which is the time derivation of the pitching motion presented in Eq. 1, time steps as long as one period  $T$  divided by 180, 360 and 720 were generated to perform the time step independency study. The hysteresis curve of the lift coefficient for all time steps is plotted in Fig. 4. It is evident that the discrepancy among the time step lengths is quite negligible and the results for the finest time steps i.e.,  $T/360$  and  $T/720$ , are so close that the curves are on top of the other. It should be noted that  $T$  stands for the time required for the completion of one period of movement which is equal to 0.49(s). As a result, the time step sizes for the implementation of this study are  $2.72 \times 10^{-3}$ ,  $1.36 \times 10^{-3}$  and  $6.8 \times 10^{-4}$  s. It should be noted that the simulations for the time step study were performed for the dry case.

### 4.3 Numerical solution validation

The numerical results obtained for the dry case, using the parameters which were proven to satisfy the independency conditions, were compared with both experimental (McAlister et al. [7]) and numerical data (Tadjfar and Asgari [31]) and presented in Fig. 5. It is evident that the numerical results could capture the trend of the aerodynamic forces as well as location of dynamic stall occurrence properly. It

**Fig. 3** Mesh generated around the airfoil

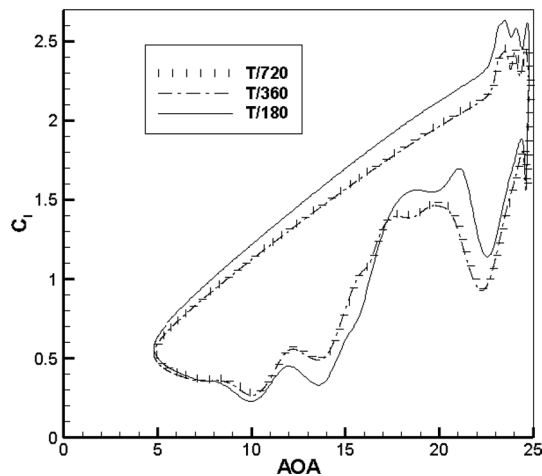
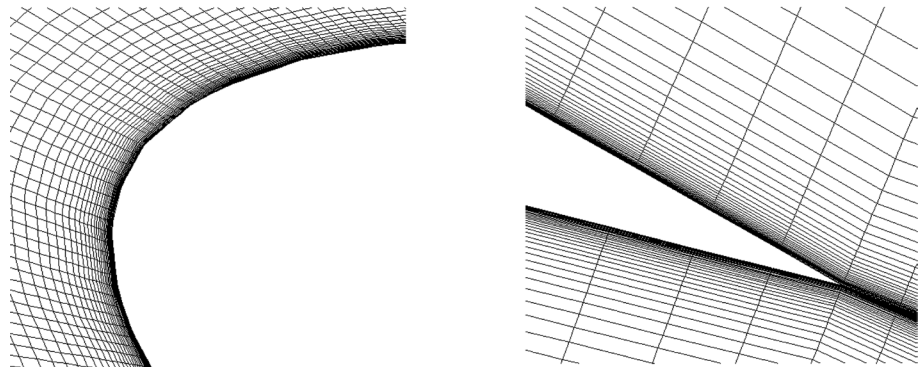
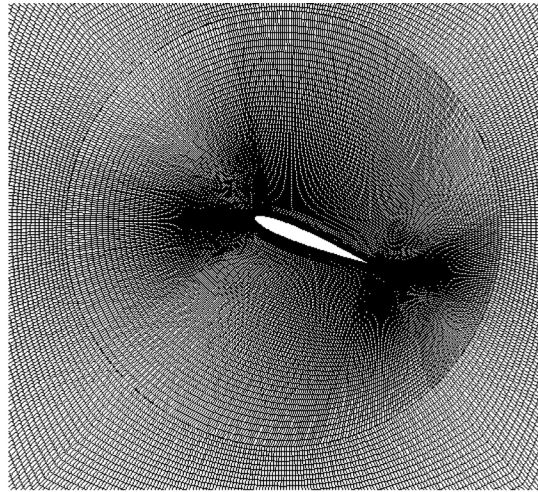


**Fig. 4** Time step study (dry case)

should be noted that there are some non-smooth changes in the experimental results indicating lack of sampling. As a result, the experimental data could not capture the lift

oscillations at the beginning of the dynamic stall, while both numerical results show some oscillations at the same angles of attack. The largest amount of difference between numerical results with the experimental data occurs during the downstroke near  $AoA = 18^\circ$ . At this point, both numerical studies fail to capture physics of dynamic stall. This point corresponds to separation of Trailing Edge Vortex (TEV) which will be discussed in details in the following sections.

As discussed in the introduction part, DPM is mainly employed as the main method for the rain simulation in different applications. In this work, in order to perform a validation study on the DPM simulation, the wet results of a static NACA-0012 airfoil at different angles of attacks were compared with that of the experimental and numerical studies conducted respectively by Bezos et al. [35] and Ismail et al. [41]. In Fig. 6 the aerodynamic coefficients of the airfoil under rainy condition have been presented. As seen in Fig. 6 the wet results of the current simulation are in a good agreement with that of the experimental work of Bezos et al. [35]. It should be noted that the same DPM settings will be used for the investigation of the rain effect on the dynamic stall.

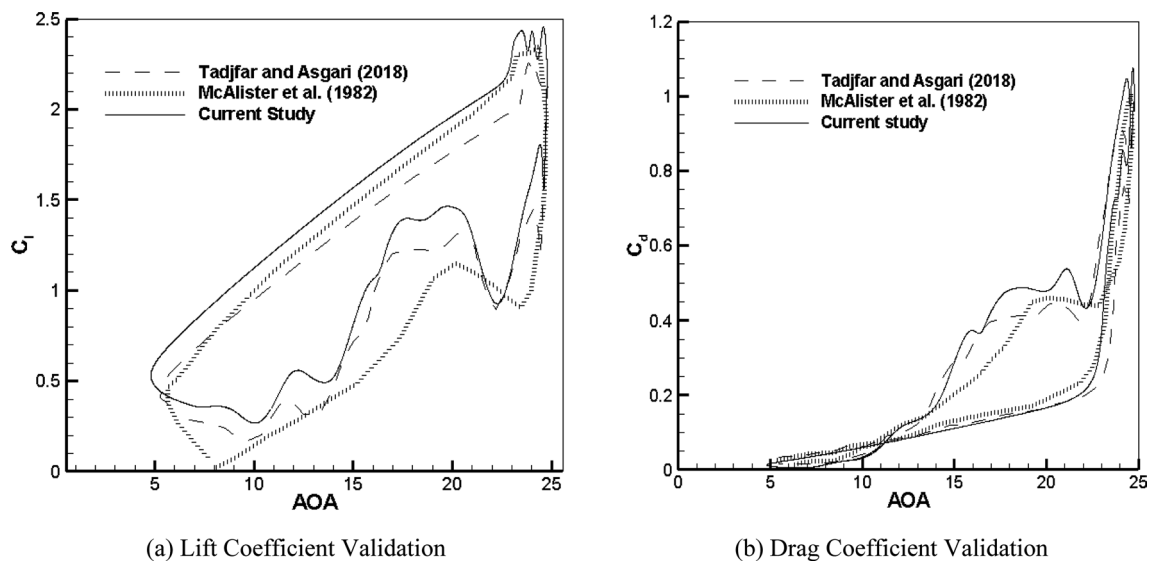


Fig. 5 Validation with experimental and numerical data in the literature (dry case)

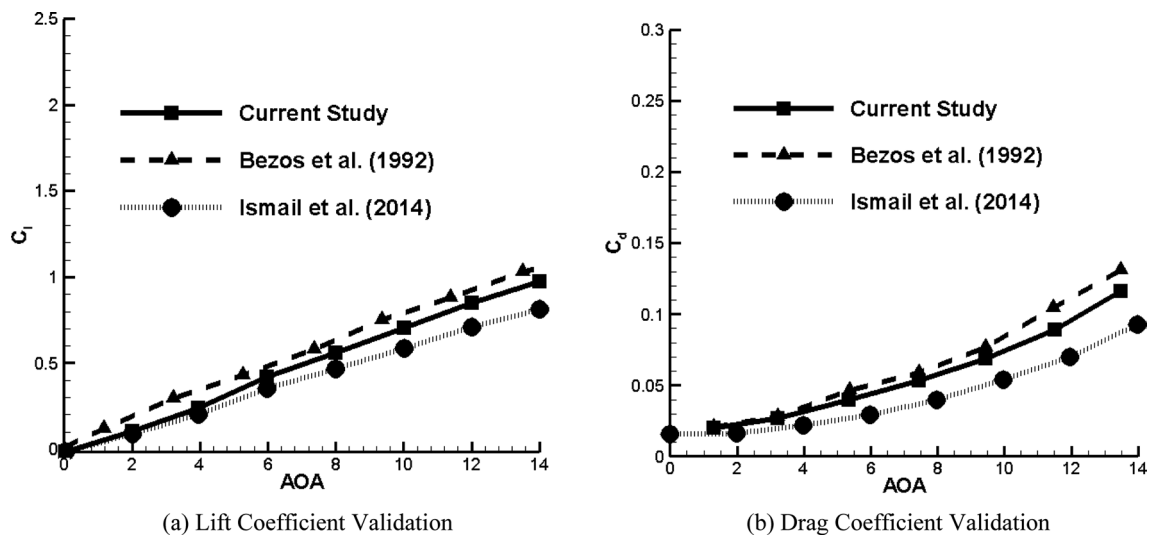


Fig. 6 Validation with experimental and numerical data in the literature (wet case)

### 4.4 Multiphase model accuracy

As mentioned at the beginning of Sect. 3, in order to find the most accurate multiphase model to predict the behavior of pitching airfoil in the rainy weather condition, DPM and DMP methods were employed. For the implementation of DPM, a two-way coupling method was utilized. Particle relaxation time is defined as follows in Eq. 14 [50]:

$$\tau = \frac{\left(\frac{\rho_p}{\rho_f} * d^2 * C_c\right)}{18\nu} \tag{14}$$

where in this study the slip correction factor,  $C_c$ , is about unity. Regarding the droplet density, air density, droplet diameter and air viscosity as  $\rho_p$ ,  $\rho_f$ ,  $d$  and  $\nu$  respectively, the relaxation time of particles will be  $3 \times 10^{-4}$ s. To be on the safe side, only three percent of the calculated relaxation time was considered as the particle time step, i.e.,  $\Delta t_p = 10^{-5}$ s. Another parameter which is required to be determined is the order of coupling. Fig. 7 demonstrates the particles coupling order in terms of volume fraction,  $\alpha_p$ , and relative relaxation time,  $\tau_p/\tau_f$  presented by Elghobashi [51]. Considering the amount of volume fraction and the relaxation time of flow and particle, this problem requires to be modeled by two-way coupling.

**Fig. 7** Classification of particle–turbulence interactions (Elghobashi [51])

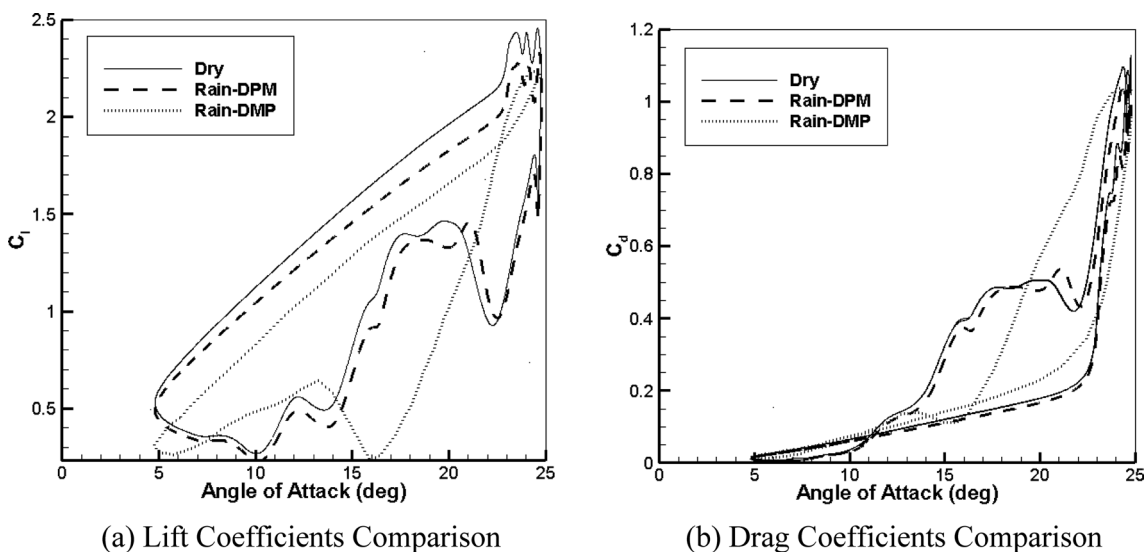
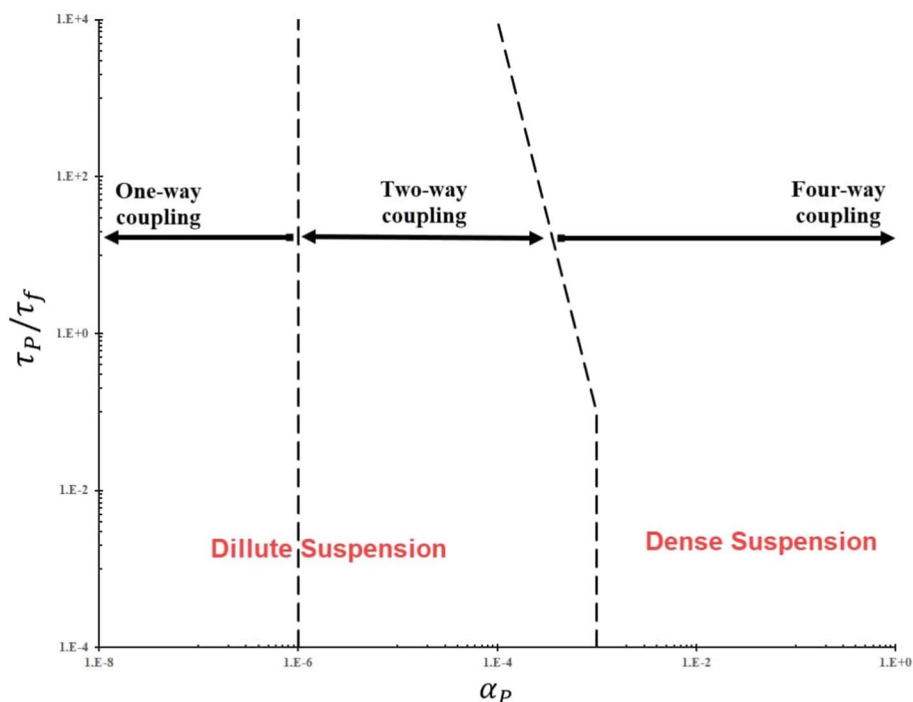


**Fig. 8** Multiphase Model accuracy investigation

In Fig. 8 the lift, drag and moment coefficients have been presented under both rainy and dry condition.

Unlike DPM, there have been few reports on utilizing Eulerian–Eulerian reference of frame for modelling raindrops in the air [52], which may be associated with the disperse nature of water drops. However, one should keep in mind that less significant deal of computational cost is imposed to the system in this method. Hence, it is wise to compare the results obtained from Eulerian–Eulerian and Eulerian–Lagrangian references of frame for simulating

water drops in air. The accuracy of the Eulerian–Lagrangian method, namely DPM, has been validated in Sect. 4.3. In addition, based on the literature, the presence of raindrops cannot make significant alterations in the trend of aerodynamic forces. However, as seen in Fig. 8, the results of the Eulerian–Eulerian method, i.e., DMP, demonstrate a totally different patterns especially at the angles of attack near the dynamic stall. Thus, the DMP method is not appropriate in capturing the physics of dynamic stall of a pitching airfoil under the rainy condition. Also, as can be observed



by looking in Fig. 8a at the lift coefficient, DMP method fails to capture the physics of dynamic stall. On the other hand, DPM demonstrates an excellent capability to yield physically meaningful results in both the pre- and post-stall conditions. Ergo, in the following steps, DPM method was chosen to study the effect of the raindrops. Also, it should be noted that the liquid water content and droplet diameter were assumed to be  $2.1\text{g/m}^3$  and  $10^{-5}\text{m}$  respectively as suggested in [53]. In addition, as [53] suggests when the We number ranges from five to ten, which is the working range of this study, the interaction between the airfoil and the raindrops is assumed to be of the rebound type.

## 5 Results and Discussion

Having evaluated the accuracy of the numerical simulation, we discuss the effect of raindrops on the aerodynamic characteristics by comparing lift and drag coefficients with those of the dry case. To achieve this goal, the lift and drag coefficient hysteresis curves of the dry and the wet cases are presented in Fig. 9. Also, to understand the physics of this phenomenon, the vorticity contours of the dry and the wet cases at different angles of attack are presented in Fig. 10. It should be noted that the points on Fig. 9 correspond to the angles of attack in Fig. 10. Also, the upwards and downwards arrows in Fig. 9 indicate upstroke and downstroke motion, respectively. As stated in Sects. 2 and 4.4, the raindrop diameter and liquid water content were set to be  $1\text{e}-5\text{m}$  and  $2.1\text{g/m}^3$ .

Overall, both the dry and wet cases follow the same trend and the overall value of the aerodynamic coefficients of the wet case is smaller than that of the dry case. Nevertheless, it is evident in Fig. 9 that there is a lead in the trend of the wet case as peaks and valleys occurred ahead of that of the dry case. Due to the fact that both cases suggest a similar trend in the lift and drag coefficient variation, in the following the aerodynamic phenomena regarding the pitching motion both in the dry and the wet case is investigated. The vorticity contours at different angles of attack during up and downstroke have been presented in Fig. 10. Figure 10a shows that at the beginning of the pitching upstroke motion the vortical structure in both cases is quite narrow. As the angle of attack increases the vortical structure begins to grow as seen in Fig. 10b. As the angle of attack rises to about 23 degrees, in Fig. 10c, the first cores of the leading-edge vortex (LEV) start to appear on the leading edge of the airfoil. It should be noted that the LEVs are typical of dynamic stall phenomenon and they come into existence due to the difference between the free stream and the leading-edge relative velocities leading to Kelvin–Helmholtz instability. Also, the presence of the LEV benefits the lift growth and it is the main responsible for the stall prognostication as it causes the velocity to increase on the suction side and at the same time decelerates the flow passing the pressure side. Obviously, by increasing the angle of attack the LEV is intensified thanks to the rise in the relative velocity between the flow and the airfoil leading edge as demonstrated in Fig. 10d. Therefore, when the angle of attack exceeds a certain limit the LEV detaches, and the lift coefficient drops dramatically as can be seen in Fig. 10e. The detachment of the LEV leads to a sharp drop in the lift coefficient and a sudden rise in the drag coefficient and this observation corresponds to the point “e” in Fig. 9. Up to this angle of attack i.e. the LEV detachment at 25 degrees, the vortical structures formation in both dry and wet cases are similar. However, straight after the LEV

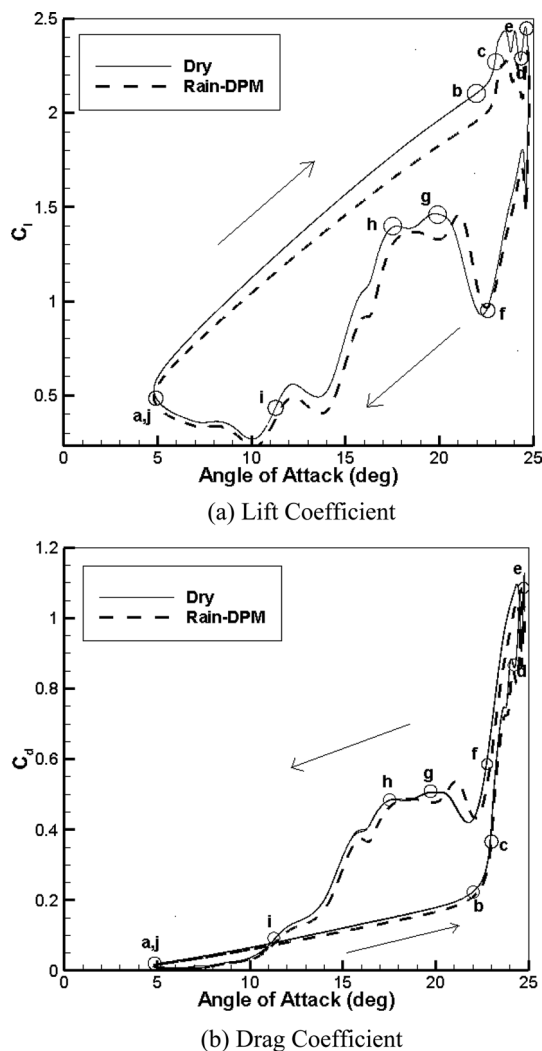
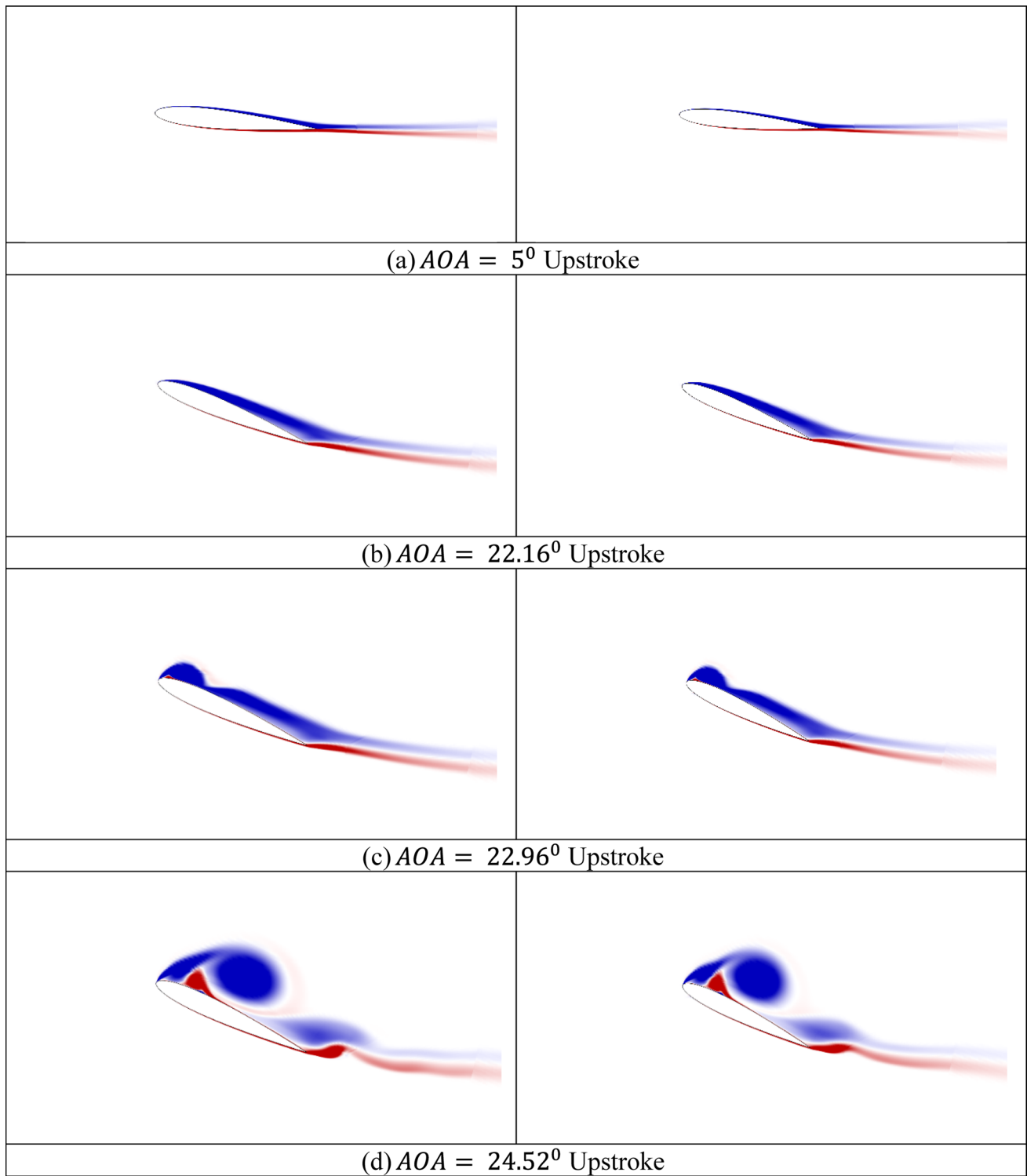


Fig. 9 Points of interest



**Fig. 10** Vorticity contours at different angles of attack (left and right contours correspond to dry and rainy condition, respectively)

detachment a lead in the formation of the vortical structures is witnessed. To illustrate, the same vortical structure reported in the wet case at  $24.79^\circ$  (Fig. 10e-right) is exactly observed in the dry case at  $22.70^\circ$  (Fig. 10f-left). Moreover,

the same trend is observed until the airfoil reaches very low angles of attacks as illustrated in Fig. 10j. Therefore, the flow separation and the succeeding phenomena, in the wet

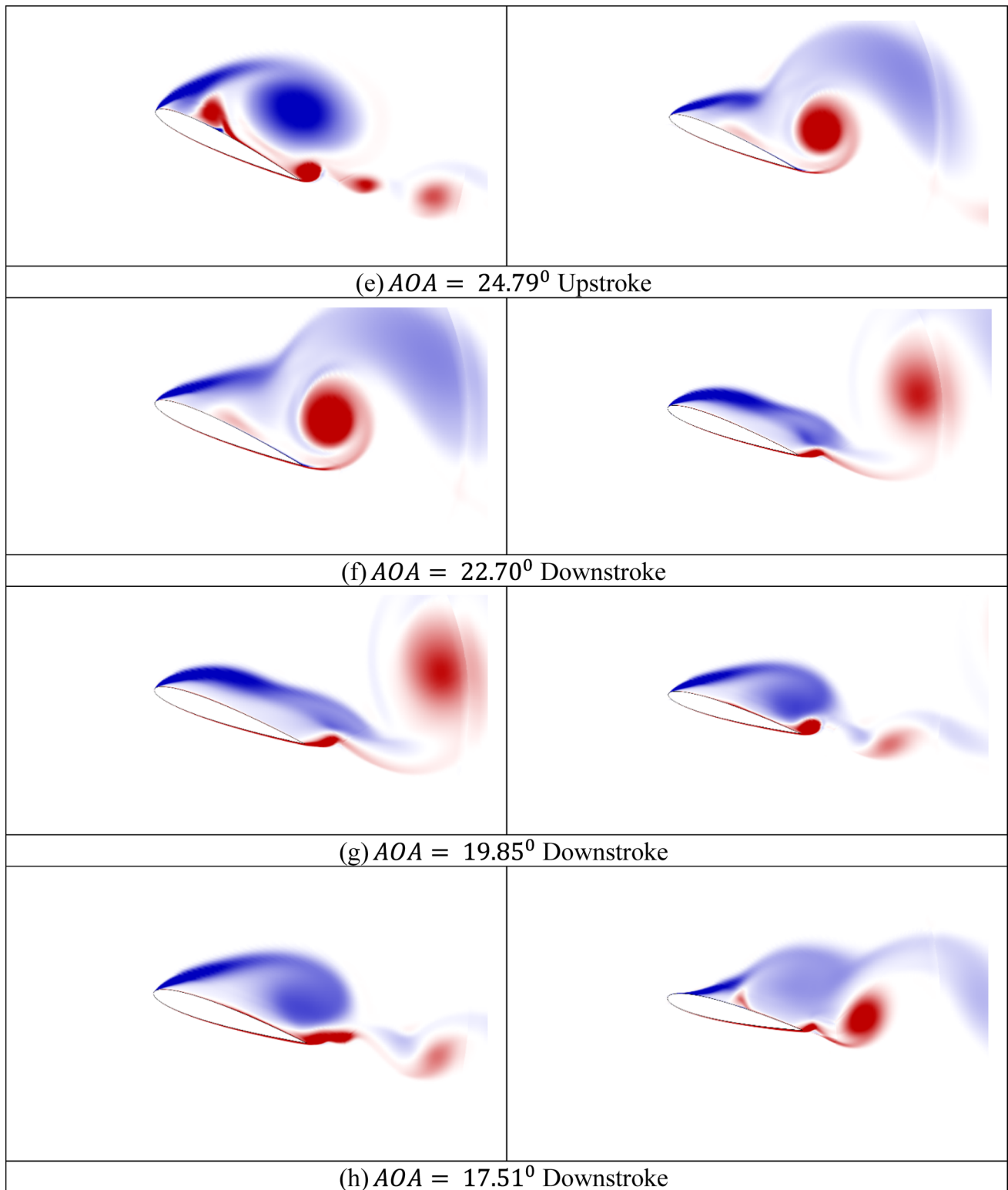


**Fig. 10** (continued)

case, happen at a lower angle of attack, during the upstroke motion, compared to the dry case.

It should also be noted that during the downstroke motion another phenomenon known as trailing edge vortex (TEV) rises into importance as the downward motion favors its

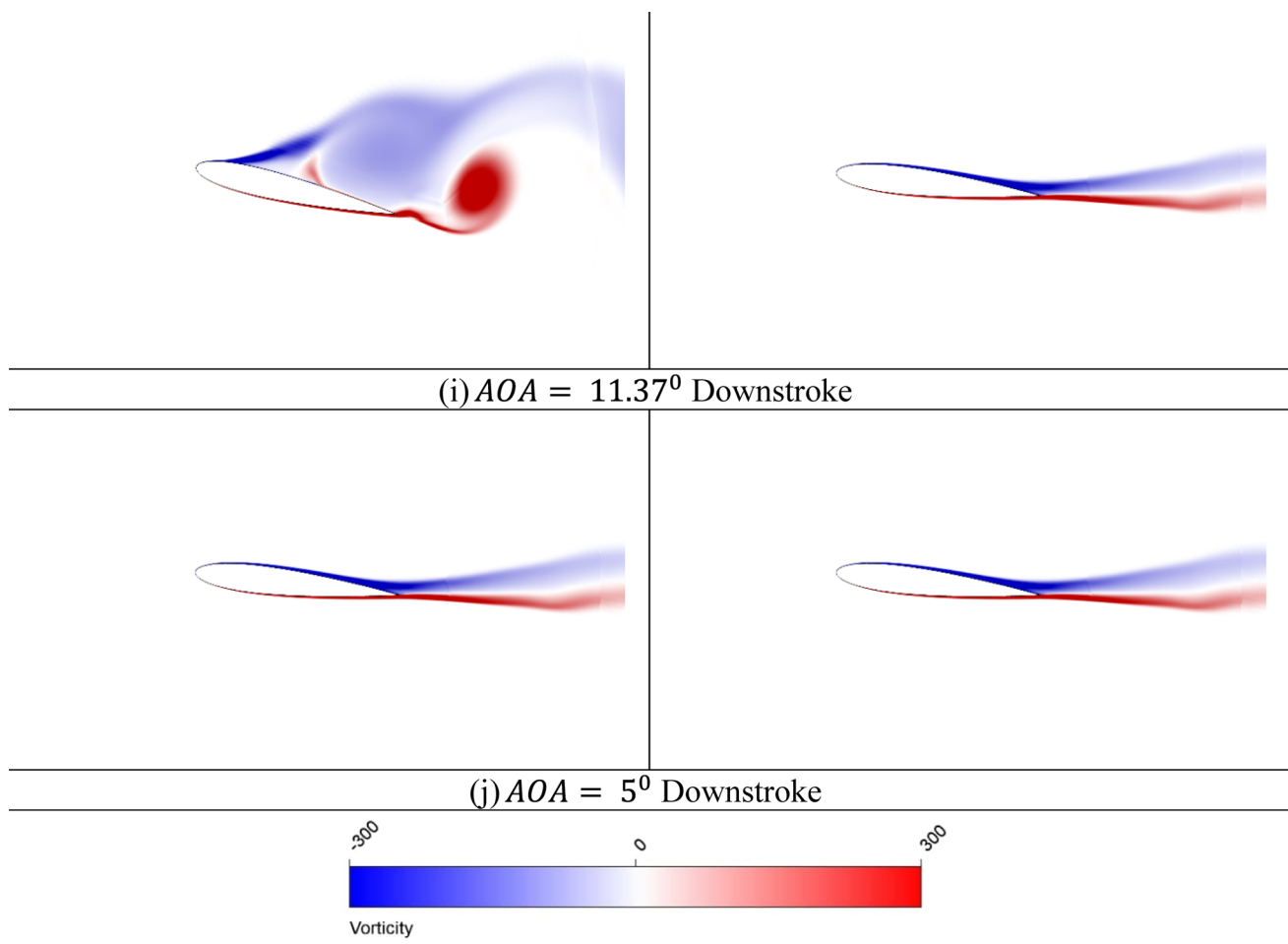
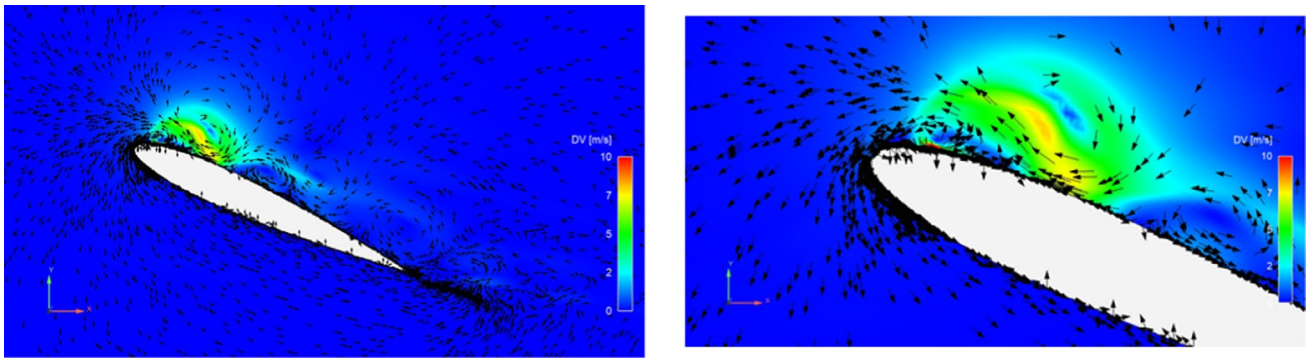


Fig. 10 (continued)

formation as a result of the velocity gradient at the trailing edge. Contrary to the LEV, TEV is a counterclockwise (CCW) vortex generated at the trailing edge of the airfoil and its formation is an adverse factor to the lift coefficient growth. This is ascribed to the fact that, because of the direction of its rotation, the TEV decelerates the flow on the suction side and accelerates the flow on the pressure side resulting in a lift drop. In order to better understand the effect of the TEV on the aerodynamic behavior of the airfoil, the vortical structures at the beginning of the TEV formation and its detachment need to be taken into consideration. To begin with, the first symptoms of the TEV formation can be observed at the beginning of the dynamic stall in Fig. 10e (shown in red) where the LEV starts to detach. A little after the LEV detachment, as demonstrated in Fig. 10f and g, the TEV grows and then detaches. Unlike the LEVs, TEV growth leads to a lift coefficient sharp drop and its detachment results in a rise in the lift coefficient as marked in Fig. 9a by the points “f” and “g”. In other words, the LEV and TEV formation and separation correspond to a

local minimum and maximum, respectively. As a result, the oscillations in the lift and drag coefficients, mainly at higher angles of attack during the downstroke motion, are due to the TEV formation and separation.

The main outcome of the description on the comparison between the vorticity contours and the aerodynamic characteristics is that the lift and drag coefficient of the rainy case is slightly lower than that of the dry case and also a lead in the aerodynamic phenomena is observed. At the first thought, these phenomena could be attributed to the lower Reynolds number of air in the wet case leading to lower amount of lift coefficient and a lead in the TEV separation. However, a numerical simulation was performed for the dry case with the air inlet velocity equal to that of the current wet case and the results showed almost the same value for the aerodynamic coefficients and with absolutely no lead or lag in their behavior. As a result, the explanation for these phenomena needs to be sought in the interaction between the primary and secondary phases. Therefore, the contour of velocity magnitude difference ( $U_{WET} - U_{DRY}$ ) between



**Fig. 11** Velocity difference between the wet and the dry case at  $AOA = 22.96^\circ$  Upstroke

the wet and the dry case along with the vectorial difference is presented in Fig. 11 to have a better understanding of the interaction. It is evident in Fig. 11 that at the leading edge the difference vectors tend downwards suggesting that the airfoil sees a lower amount of angle of attack which corresponds to a lower amount of lift coefficient. Also, at the trailing edge, the difference vectors show a TEV like vortical structure. As discussed earlier, the presence of a CCW vortex at the trailing edge has an adverse effect on the lift generation of the pitching airfoil which is one of the mechanisms leading to a lower amount of lift coefficient of the wet case compared to the dry case. Further, regarding the vector differences, it is evident in Fig. 11 that the flow in the suction side experiences a deceleration, while on the pressure side it accelerates. In other words, an LEV with an unfavorable rotation direction (CCW) is seen at the leading edge. All the observations from Fig. 11 imply that due to the two-way coupling the air velocity vectors of the upstream flow undergoes an alteration due to the forces exerted by the secondary phase.

## 6 Conclusion and summary

In this study the effect of raindrops on the dynamic stall of a NACA-0012 pitching airfoil at a Reynolds number equal to  $10^6$  was investigated. The well-known  $k - \omega$ SST model was utilized to account for the turbulent phenomena. In addition, to exploit the maximum accuracy of this model,  $y^+ \sim 1$  was considered for the airfoil boundary. The rain condition was set as suggested in [53]. Hence, the raindrop diameters and liquid water content were set  $10^{-5}$  m and  $2.1 \text{ g/m}^3$ , respectively. To implement an accurate two-phase study two different well-known models were compared and the most accurate one called Discrete Phase Model (DPM) was selected as the main two-phase model. It was shown that the Disperse Multiphase (DMP) method is not capable

of capturing the physics of the dynamic stall. As a result, DPM was employed to investigate the effect of raindrops on the pitching airfoil. Furthermore, to ensure the accuracy of the numerical results, the grid and time step independency were implemented, respectively. In the end, the numerical solution was validated against an experimental [7] and a numerical [31] studies.

The comparison between the lift and drag coefficients revealed that a lead and drop in both the coefficients occurred. More precisely, wet condition phenomena occurred in advance of that of the dry one with slightly lower magnitude. Firstly, it was discussed that Reynolds number does not play a pivotal role in the lift reduction or phase lead as the hysteresis curves of the aerodynamic coefficients for the dry cases with the inlet velocity being equal to the main dry case and the wet case were stated to be very close in value and no phase shift was observed. Secondly, the two-way coupling of air and raindrops, causes the flow to undergo an alteration in its direction near the leading edge. The velocity difference contours proved the direction of velocity in the rainy case lies in the adverse direction, as a result of two-way coupling, which leads to a lower amount of aerodynamic coefficients in general. The vorticity contours of the dry and the wet cases showed that the Leading Edge Vortex (LEV) and Trailing Edge Vortex (TEV) of the wet case tend to separate anterior to the dry case. Also, it was illustrated that the LEV formation contributed to lift augmentation, while the presence of TEV results in a reduction in the lift coefficient. Hence, their separation counteracts their positive or negative effects on the aerodynamic coefficients to a considerable extent. Therefore, to sum up, the main findings of this study are as follows:

- DPM is a more accurate solution for modelling raindrops effects on a pitching airfoil than DMP is. Since the latter has been proven to be not able to capture the physics of the flow.

- Raindrops cause a reduction in the magnitude of lift and drag coefficients.
- Raindrops do not alter the main trend of the aerodynamic coefficients but they bring a lead in the trend.
- The lower Reynolds number of the wet case was shown not to have a considerable effect on the lower amount of the aerodynamic coefficients and phase shift.
- The two-way coupling between the primary and the secondary phases was found to change the local angle of attack affecting the aerodynamic of the airfoil.
- The interaction between the primary and secondary phases was found to be the most important factor resulting in the observed phenomena.

**Funding** Open access funding provided by Politecnico di Milano within the CRUI-CARE Agreement.

**Open Access** This article is licensed under a Creative Commons Attribution 4.0 International License, which permits use, sharing, adaptation, distribution and reproduction in any medium or format, as long as you give appropriate credit to the original author(s) and the source, provide a link to the Creative Commons licence, and indicate if changes were made. The images or other third party material in this article are included in the article's Creative Commons licence, unless indicated otherwise in a credit line to the material. If material is not included in the article's Creative Commons licence and your intended use is not permitted by statutory regulation or exceeds the permitted use, you will need to obtain permission directly from the copyright holder. To view a copy of this licence, visit <http://creativecommons.org/licenses/by/4.0/>.

## References

1. Yeznasni A, Derdelinckx R, Hirsch C (1992) Influence of dynamic stall in the aerodynamic study of HAWTs. *J Wind Eng Ind Aerodyn* 39:187–198. [https://doi.org/10.1016/0167-6105\(92\)90545-L](https://doi.org/10.1016/0167-6105(92)90545-L)
2. Buchner AJ, Lohry MW, Martinelli L et al (2015) Dynamic stall in vertical axis wind turbines: comparing experiments and computations. *J Wind Eng Ind Aerodyn* 146:163–171. <https://doi.org/10.1016/j.jweia.2015.09.001>
3. Antonini EGA, Bedon G, De BS et al (2015) Innovative discrete-vortex model for dynamic stall simulations. *AIAA J* 53:1–7. <https://doi.org/10.2514/1.J053430>
4. Dyachuk E, Goude A, Bernhoff H (2014) Dynamic stall modeling for the conditions of vertical axis wind turbines. *AIAA J* 52:72–81. <https://doi.org/10.2514/1.J052633>
5. Sheng W, Galbraith RAM, Coton FN (2013) Prediction of dynamic stall onset for oscillatory low-speed airfoils. *J Fluids Eng* 130:1–8. <https://doi.org/10.1115/1.2969450>
6. Trembley-Dionne V, Lee T (2019) Effect of trailing-edge flap deflection on a symmetric airfoil over a wavy ground. *J Fluids Eng* 141:12–15. <https://doi.org/10.1115/1.4041736>
7. McAlister KW, Pucci SL, McCroskey WJ, Carr LW (1982) An experimental study of dynamic stall on advanced airfoil sections volume 2. pressure and force data. NASA Ames Research Center, Moffett Field, CA
8. Wang Q, Zhao Q (2016) Experiments on unsteady vortex flow-field of typical rotor airfoils under dynamic stall conditions. *Chin J Aeronaut* 29:358–374. <https://doi.org/10.1016/j.cja.2016.02.013>
9. Leknys RR, Arjomandi M, Kelso RM, Birzer CH (2018) Thin airfoil load control during post-stall and large pitch angles using leading-edge trips. *J Wind Eng Ind Aerodyn* 179:80–91. <https://doi.org/10.1016/j.jweia.2018.05.009>
10. Seyednia M, Masdari M, Vakili-pour S (2019) The influence of oscillating trailing-edge flap on the dynamic stall control of a pitching wind turbine airfoil. *J Brazilian Soc Mech Sci Eng* 41:1–15. <https://doi.org/10.1007/s40430-019-1693-z>
11. Pourmostafa M, Ghadimi P (2018) Investigating the interaction of two oscillating foils in tandem arrangement, using 3D unsteady boundary element method. *J Brazilian Soc Mech Sci Eng* 40:1–24. <https://doi.org/10.1007/s40430-018-1323-1>
12. Karimian SMH, Aramian SV, Abdolahifar A (2021) Numerical investigation of dynamic stall reduction on helicopter blade section in forward flight by an airfoil deformation method. *J Brazilian Soc Mech Sci Eng* 43:1–17. <https://doi.org/10.1007/s40430-021-02822-y>
13. Hadidoolabi M, Ansarian H (2018) Computational investigation of vortex structure and breakdown over a delta wing at supersonic pitching maneuver. *J Brazilian Soc Mech Sci Eng* 40:1–17. <https://doi.org/10.1007/s40430-018-1021-z>
14. Bouzاهر MT, Hadid M, Semch-Eddine D (2017) Flow control for the vertical axis wind turbine by means of flapping flexible foils. *J Brazilian Soc Mech Sci Eng* 39:457–470. <https://doi.org/10.1007/s40430-016-0618-3>
15. Angulo IA, Ansell PJ (2019) Influence of aspect ratio on dynamic stall of a finite wing. *AIAA J* 57:2722–2733. <https://doi.org/10.2514/1.J057792>
16. Ouro P, Stoesser T, Ram L (2018) Effect of blade cambering on dynamic stall in view of designing vertical axis turbines. *J Fluids Eng* 140:1–12. <https://doi.org/10.1115/1.4039235>
17. Leknys RR, Arjomandi M, Kelso RM, Birzer CH (2019) Dynamic stall flow structure and forces on symmetrical airfoils at high angles of attack and rotation rates. *J Fluids Eng* 141:1–15. <https://doi.org/10.1115/1.4041523>
18. Mariappan S, Gardner AD, Richter K, Raffel M (2014) Analysis of dynamic stall using dynamic mode decomposition technique. *AIAA J* 52:2427–2439. <https://doi.org/10.2514/1.J052858>
19. Algozino S, Maranon L, Delnero J, Capittini G (2018) Turbulence effect on flat plate pitching airfoil. In: *AIAA AVIATION Forum, Fluid Dynamics Conference*, pp 1–11
20. Merrill BE, Peet YT (2017) Effect of impinging wake turbulence on the dynamic stall of a pitching airfoil. *AIAA J* 55:4094–4112. <https://doi.org/10.2514/1.J055405>
21. Ansell P, Mulleners K (2019) Multiscale vortex characteristics of dynamic stall from empirical mode decomposition. *AIAA J* 58:1–18. <https://doi.org/10.2514/1.J057800>
22. Visbal MR, Garmann DJ (2019) Dynamic stall of a finite-aspect-ratio wing. *AIAA J* 57:1–16. <https://doi.org/10.2514/1.J057457>
23. Wang L, Fu S (2017) Detached-eddy simulation of flow past a pitching NACA 0015 airfoil with pulsed actuation. *Aerosp Sci Technol* 69:123–135. <https://doi.org/10.1016/j.ast.2017.06.002>
24. Tadjfar M, Asgari E (2018) The role of frequency and phase difference between the flow and the actuation signal of a tangential synthetic jet on dynamic stall flow control. *J Fluids Eng* 140:1–13. <https://doi.org/10.1115/1.4040795>
25. Yen J, Ahmed NA (2013) Parametric study of dynamic stall flow field with synthetic jet actuation. *J Fluids Eng* 134:1–8. <https://doi.org/10.1115/1.4006957>
26. Singhal A, Castañeda D, Webb N, Samimy M (2017) Control of Dynamic Stall over a NACA 0015 airfoil using plasma actuators. *AIAA J* 56:1–12. <https://doi.org/10.2514/1.J056071>

27. De Giorgi MG, Motta V, Suma A (2020) Influence of actuation parameters of multi-DBD plasma actuators on the static and dynamic behaviour of an airfoil in unsteady flow. *Aerosp Sci Technol* 96:1–13. <https://doi.org/10.1016/j.ast.2019.105587>
28. Lombardi AJ, Bowles PO, Corke TC et al (2013) Closed-loop dynamic stall control using a plasma actuator. *AIAA J* 51:1130–1141. <https://doi.org/10.2514/1.J051988>
29. Zhao Q, Ma Y, Zhao G (2017) Parametric analyses on dynamic stall control of rotor airfoil via synthetic jet. *Chin J Aeronaut* 30:1818–1834. <https://doi.org/10.1016/j.cja.2017.08.011>
30. Liu J, Chen R, Qiu R et al (2020) Study on dynamic stall control of rotor airfoil based on coflow jet. *Int J Aerosp Eng*. <https://doi.org/10.1155/2020/8845924>
31. Tadjfar M, Asgari E (2018) Active flow control of dynamic stall by means of continuous jet flow at reynolds number. *J Fluids Eng* 140:1–10. <https://doi.org/10.1115/1.4037841>
32. Rhode R (1941) Some effects of rainfall on flight of airplanes and on instrument indications. NASA Tech Reports
33. LUERS J (1983) Heavy rain effects on aircraft. 21st Aerosp Sci Meet 2015–2023. <https://doi.org/10.2514/6.1983-206>
34. Hess CF, Li F (1987) Optical technique to characterize heavy rain. *Aerosp Eng*, pp 1–6. <https://doi.org/10.2514/6.1986-292>
35. Bezos G, Dunham R, Gentry G, Meldon E (1992) Wind tunnel aerodynamic characteristics of a transport-type airfoil in a simulated heavy rain environment. NASA Tech Reports
36. Bezos G, Dunham R, Gentry G, Melson Jr W (1987) Wind tunnel test results of heavy rain effects on airfoil performance. <https://doi.org/10.2514/6.1987-260>
37. Thompson BE, Jang J, Dion JL (1995) Wing performance in moderate rain. *J Aircr* 32:1034–1039. <https://doi.org/10.2514/3.46833>
38. Valentine JR, Decker RA (1995) A Lagrangian-Eulerian scheme for flow around an airfoil in rain. *Int J Multiph Flow* 21:639–648
39. Wu Z, Cao Y, Ismail M (2013) Numerical simulation of airfoil aerodynamic penalties and mechanisms in heavy rain. *Int J Aerosp Eng* 2013:1–13. <https://doi.org/10.1155/2013/590924>
40. Wu Z, Cao Y (2015) International Journal of Multiphase Flow Numerical simulation of flow over an airfoil in heavy rain via a two-way coupled Eulerian-Lagrangian approach. *Int J Multiph FLOW* 69:81–92. <https://doi.org/10.1016/j.ijmultiphaseflow.2014.11.006>
41. Ismail M, Yihua C, Wu Z, Sohail MA (2014) Numerical study of aerodynamic efficiency of a wing in simulated rain environment. *J Aircr* 51:2015–2023. <https://doi.org/10.2514/1.C032594>
42. Fatahian H, Salarian H, Eshagh Nimvari M, Khaleghinia J (2020) Effect of Gurney flap on flow separation and aerodynamic performance of an airfoil under rain and icing conditions. *Acta Mech Sin Xuebao* 36:659–677. <https://doi.org/10.1007/s10409-020-00938-3>
43. Fatahian H, Salarian H, Nimvari ME, Khaleghinia J (2020) Computational fluid dynamics simulation of aerodynamic performance and flow separation by single element and slatted airfoils under rainfall conditions. *Appl Math Model* 83:683–702. <https://doi.org/10.1016/j.apm.2020.01.060>
44. Fatahian H, Salarian H, Eshagh Nimvari M, Khaleghinia J (2020) Numerical simulation of the effect of rain on aerodynamic performance and aeroacoustic mechanism of an airfoil via a two-phase flow approach. *SN Appl Sci* 2:1–16. <https://doi.org/10.1007/s42452-020-2685-4>
45. Cai M, Abbasi E, Arastoopour H (2013) Analysis of the performance of a wind-turbine airfoil under heavy-rain conditions using a multiphase computational fluid dynamics approach. *Ind Eng Chem Res* 52:3266–3275. <https://doi.org/10.1021/ie300877t>
46. Cohan AC, Arastoopour H (2016) Numerical simulation and analysis of the effect of rain and surface property on wind-turbine airfoil performance. *Int J Multiph Flow* 81:46–53. <https://doi.org/10.1016/j.ijmultiphaseflow.2016.01.006>
47. Wu Z, Cao Y, Nie S, Yang Y (2017) Effects of rain on vertical axis wind turbine performance. *J Wind Eng Ind Aerodyn* 170:128–140. <https://doi.org/10.1016/j.jweia.2017.08.010>
48. Jian DU, Xi-feng L, Gui-bo LI (2020) Numerical simulatim of rainwater accumulation and flow characteristics over windshield of high-speed trains. *J Cent South Univ* 200–209
49. Yu M, Liu J, Dai Z (2021) Aerodynamic characteristics of a high-speed train exposed to heavy rain environment based on non-spherical raindrop. *J Wind Eng Ind Aerodyn* 211:104532. <https://doi.org/10.1016/j.jweia.2021.104532>
50. Zhang J, Li A (2008) CFD simulation of particle deposition in a horizontal turbulent duct flow. *Chem Eng Res Des* 86:95–106. <https://doi.org/10.1016/j.cherd.2007.10.014>
51. Elghobashi S (1991) Particle-laden turbulent flows: direct simulation and closure models. *Appl Sci Res* 48:301–314. <https://doi.org/10.1007/BF02008202>
52. Han W, Kim J, Kim B (2018) Study on correlation between wind turbine performance and ice accretion along a blade tip airfoil using CFD. *J Renew Sustain Energy* 10. <https://doi.org/10.1063/1.5012802>
53. Wu Z, Cao Y (2016) Numerical simulation of airfoil aerodynamic performance under the coupling effects of heavy rain and ice accretion. *Adv Mech Eng* 8:1–9. <https://doi.org/10.1177/1687814016667162>

**Publisher's Note** Springer Nature remains neutral with regard to jurisdictional claims in published maps and institutional affiliations.